Tribology International 43 (2010) 1087–1090

Contents lists available at ScienceDirect

Tribology International

journal homepage: www.elsevier.com/locate/triboint

A novel tribometer for the measurement of friction in MEMS

I.S.Y. Ku [a,*], T. Reddyhoff [a], J.H. Choo [a,1], A.S. Holmes [b], H.A. Spikes [a]

[a] Department of Mechanical Engineering, Imperial College London, London SW7 2AZ, UK
[b] Department of Electrical and Electronic Engineering, Imperial College London, London SW7 2AZ, UK

ARTICLE INFO

Available online 21 December 2009

Keywords:
Micro-electro-mechanical systems (MEMS)
Lubrication
Friction
Tribometer
Microtribology

ABSTRACT

A new tribometer has been developed to determine friction under conditions that are representative of MEMS (micro-electro-mechanical-systems). The tribometer consists of a rotating silicon disc, loaded against a stationary silicon disc. Friction and film thickness values are measured using laser displacement techniques. In this study, two different test set-ups were used: a flat on flat specimen geometry, and a moving flat against a structured surface, similar to that of a miniature thrust pad bearing. Using this tribometer, hydrodynamic tests have been carried out with the specimens fully submerged in hydrocarbon lubricants. Results suggest that friction increases with sliding speed and decreases with increasing applied normal load, which is in accordance with the hydrodynamic theory.

1. Introduction

MEMS technology is central to a number of engineering products, including inertial sensors, inkjet printer heads and digital micromirror displays. A common feature of these devices, and of other successful MEMS products, is that they do not contain any sliding contacts. The difficulty of lubricating small, high sliding parts currently makes MEMS with large amounts of sliding impracticable. Unfortunately the lubrication regimes in the macroscale cannot be directly transferred to the microscale, primarily because the large surface area to volume ratio means that surface forces outweigh the effects of inertia. These problems have led to a range of MEMS tribometers being built over the years to explore MEMS friction and wear [1–4].

Various methods have been applied to reduce friction and wear in MEMS. The majority of these involve surface treatments such as hydrogen termination [5]. Another common approach is the deposition on MEMS surfaces of self-assembled monolayers (SAMs) from liquids [6]. However, the resistance of such monolayers to wear is low when the load is high [6]. It has been shown recently that effective lubricant films for MEMS can be produced and replenished via the vapour phase [7]. Liquid-based hydrodynamic lubrication is generally ignored in MEMS, as the drag is presumed to be so large that the moving parts are 'overdamped' [8]. A study had attempted to operate electrostatic micromotors in a liquid environment, and this was successful with liquids with different dielectric constants [9]. Nainaparamphil et al. [10] demonstrated the use of ionic liquids to lubricate MEMS with high sliding conditions (MEMS motor devices); it was found that, with the lubrication, the number of cycles to failure was about 20 times higher than for unlubricated surfaces.

This study involves the development of a tribometer to explore and investigate suitable methods for lubricating high sliding MEMS. Macroscale experience suggests that lubrication is generally most effective if the lubricating film can be continually replenished during use. Therefore, one aim in the longer term is to explore the use of various self-replenishment mechanisms in the lubrication of MEMS.

2. Experimental details

A new tribometer has been developed which allows friction results to be obtained for mm-scale MEMS specimens rubbed together under high sliding conditions. In the present work the specimens are silicon discs with a diameter of 2 mm, fabricated by deep reactive ion etching (DRIE). The upper disc is attached to a rotating shaft, while the lower is mounted on a stationary platform. The latter is supported by a system of elastic suspension beams, also formed by silicon DRIE, which allows limited rotation about the vertical axis and also limited vertical displacement. A schematic diagram is shown in Fig. 1. The upper sample is attached to the motor shaft via a self-aligning mechanism, which operates in a similar fashion to a flexible coupling between the upper sample and the motor. This mechanism involves a ball-joint with pins which accommodates a small rotation about an axis at 90° to that of the motor rotation. This compensates for any slight misalignment between the motor shaft and the lower specimen. The specimen is held in place by a holding force between a

* Corresponding author.
E-mail address: ingrid.ku@imperial.ac.uk (I.S.Y. Ku).
[1] Now with the Department of Mechanical Engineering, National University of Singapore, 9 Engineering Drive 1, Singapore 117576, Singapore.

0301-679X/$ - see front matter © 2009 Elsevier Ltd. All rights reserved.
doi:10.1016/j.triboint.2009.12.029

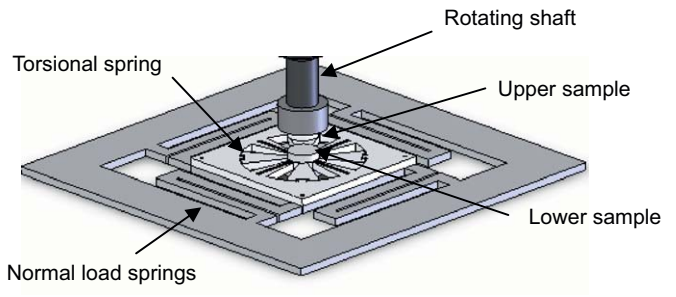

Fig. 1. A schematic of the contacting parts. (Drawing created in Solidworks Educational Edition)

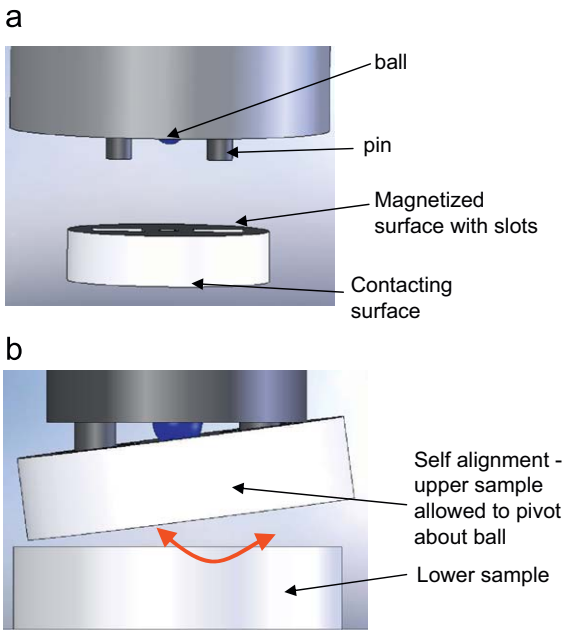

Fig. 2. Illustration of self-alignment mechanism. (a) Unassembled. (b) Assembled. (Drawings created in Solidworks Educational Edition)

magnet, located on the motor shaft and a nickel coating on the specimen surface. An illustration is shown in Fig. 2.

During testing, the upper specimen is rotated and the resulting, very small, rotational displacement of the lower specimen is measured using a light lever technique. A laser beam is deflected from a small, reflective prism mounted beneath the platform to a controlled piezoelectric actuator, before being deflecting off four stationary mirrors, and finally being incident on the surface of a light-detecting sensor. The path of the laser beam is shown in Fig. 3. A control loop is set up between the light sensor and piezoelectric actuator such that the laser beam is always incident on the same region of the detector. Thus the voltage signal to the piezoelectric actuator can be calibrated against rotational displacement of the lower specimen. The sensitivity of the method is increased by the large distance between the actuator and sensor, generated by the four mirrors.

The upper specimen and motor are attached to an accurate ($\pm 0.1\,\mu m$) computer-controlled stage. Normal loading of the specimens is achieved by the controlled motion of this stage. The vertical displacement of the lower specimen is measured using a laser displacement device mounted below the platform. The platform stiffnesses are calibrated to enable the normal load and frictional torque to be obtained from the displacement measurements. Normal load calibration is carried out by placing known weights on the platform and measuring the corresponding vertical deflections using the laser displacement measurement device. This is illustrated in Fig. 4. Eq. (1) shows the relation between the displacement and the normal load, where N is the normal load, x is the displacement and k_1 is the stiffness. For the torque calibration, a custom-made device is used to apply known torques by means of two beams with strain gauges attached to the platform. Eq. (2) shows the relation between the angular displacement and the torque, where T is the torque, k_2 is the torsional stiffness and ϕ is the angular displacement.

$$N = k_1 x \tag{1}$$

$$T = k_2 \phi \tag{2}$$

In experiments, the upper sample is brought into contact with the lower sample. Then a known normal load is applied, and measured by the laser displacement unit. This displacement of the lower platform determines the initial normal applied load. Two types of contact geometry have been studied. One uses both samples having flat, contacting surfaces; the other has the upper sample with a flat surface but the lower sample with a structured one. The patterns on the structured samples are etched to a depth of 50 μm using DRIE to form sector-shaped pads with various configurations. Fig. 5 shows images of the structured samples used in the tests. These consist of separate and linked raised pads separated by etched regions, arranged circumferentially around the sample centre. The use of DRIE enables a wide range of pad geometries to be manufactured very easily and repeatably.

A DC voltage is applied to the motor and the rotating speed is monitored via an attached encoder. The vertical displacement and rotational displacement of the platform are measured at each speed throughout the test, from which friction and film thicknesses are obtained, respectively.

For viscous lubricants, the lubricant film thickness during testing can be measured from the change in vertical position of the platform. This measurement is made using the laser displacement device beneath the platform (which is also used to measure normal load). It is assumed that the initial film thickness, immediately after application of the normal load, is zero. This is in accordance to squeeze film theory, where the film thickness reaches a value equivalent to the roughness of the surface within a few milliseconds of being loaded. The upper sample is mounted on the motor shaft, which is assumed to be rigid, so the change in the vertical position of the lower sample platform during the test can be taken as a direct measure of the film thickness. It is important to note that, as the film thickness increases, this further deflects the platform suspension resulting in a progressive increase in the load experienced by the bearing, which is the sum of the initial applied load and that due to deflection due to film formation.

The initial applied load during the tests ranges from 0.01 to 0.2 N and sliding rotational speeds are in the range 1200–30 000 rpm. In the initial testing work described in this paper, lubrication has been achieved by submerging the contact in the hydrocarbon liquid squalane. Squalane was selected as it is a pure hydrocarbon with a sufficient viscosity to generate relatively thick hydrodynamic films, without the aid of additives. Many hydrocarbons with high molecular weights are solid at room temperature, but the branched chain structure of squalane means that it is allowed to remain at liquid state at room temperature. It should be noted that we do not consider squalane to be an appropriate liquid lubricant for actual MEMS devices. Lower viscosity fluids appear more appealing and are currently being tested. However, a viscous fluid was chosen to fully explore the capability of the new test rig.

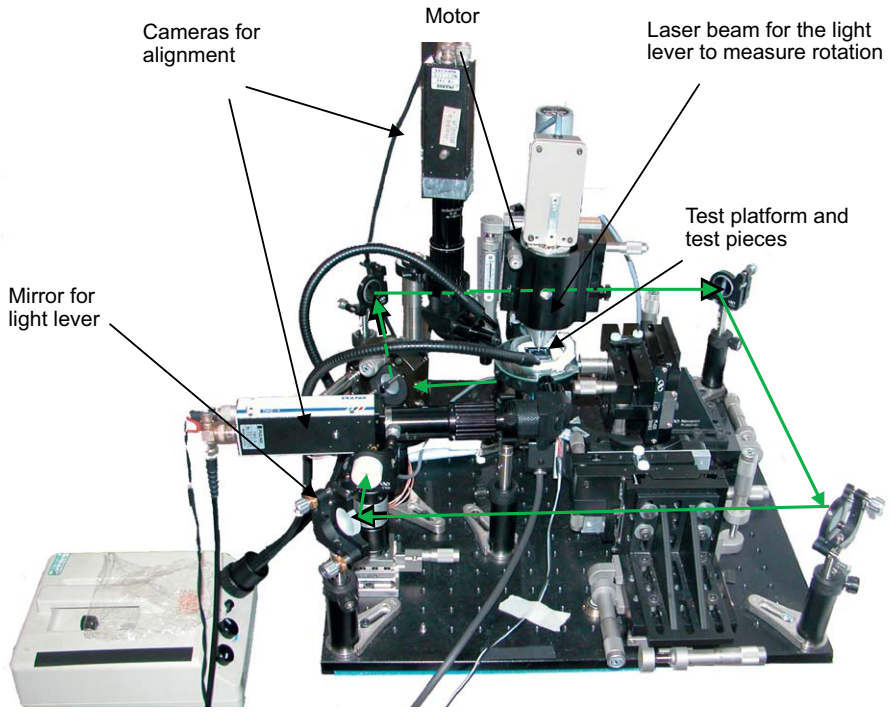

Fig. 3. Photograph of the test rig, with the path of the light lever highlighted in green. (For interpretation of the references to colour in this figure legend, the reader is referred to the web version of this article.)

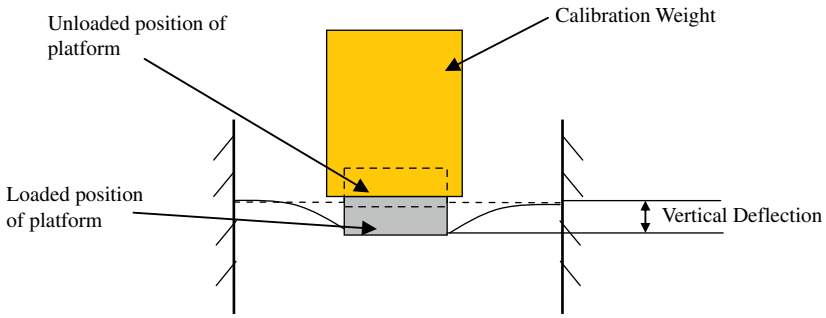

Fig. 4. Illustration of the measurement and calibration of the normal load.

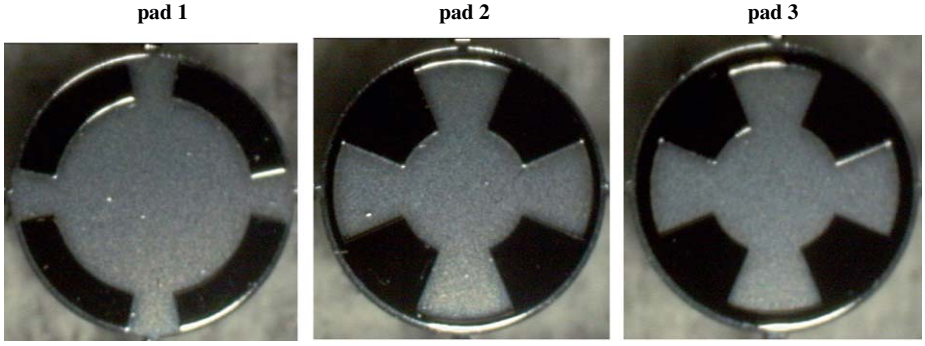

Fig. 5. Photographs of structured samples (the pale regions correspond to the regions where the wafer has been etched away, while the dark regions are protruding pads).

3. Results and discussion

3.1. Friction

Fig. 6 shows how measured friction varies with rotational speed. It can be seen that the tests using the structured surfaces exhibit lower values of friction than those where the surfaces are flat. Friction increases with speed, showing that the contact is operating in the hydrodynamic regime—since friction is arising from increased shearing of the fluid. No increase in friction at low speeds due to the observation of high boundary friction, down to the lowest attainable motor speed.

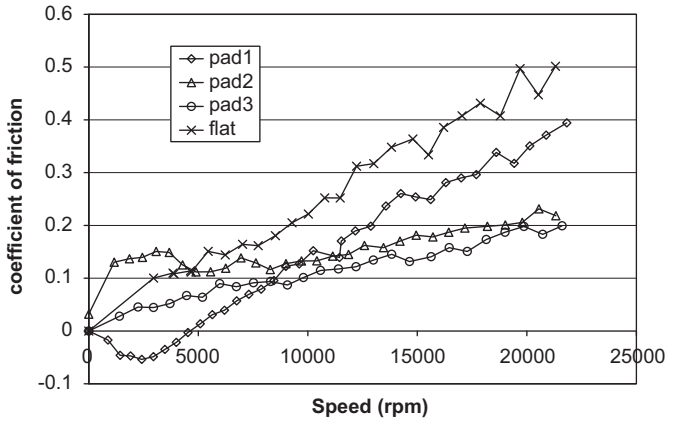

Fig. 6. Friction results for the flat on flat and the flat on textured surfaces compared (pads 1–3 indicate different patterns on the structured surfaces).

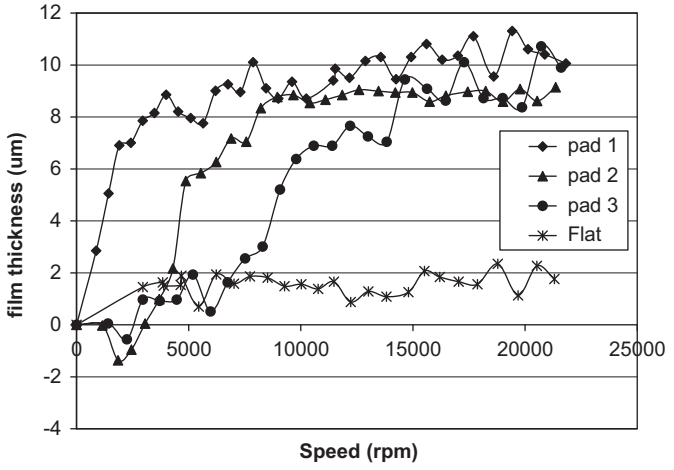

Fig. 7. Film thickness results for the flat on flat and the flat on textured surfaces compared (pads 1–3 indicate different patterns on the structured surfaces).

3.2. Film thickness measurements

The vertical position of the lower sample is monitored throughout the tests, and this can be used to evaluate the film thickness. Large changes in film thickness occurred in the tests with the textured surfaces, as shown in Fig. 7. Hydrodynamic theory predicts that the fluid film thickness is wholly dependent on the bearing convergence (i.e. ratio of inlet to outlet thickness). The textured pads with finite convergence give much thicker films than parallel smooth pads, where convergence exists only from misalignment or thermal effects. Entrainment of lubricant into this converging geometry causes a pressure to develop between the pads allowing the lubricant film to support a load. As a result, the film thickness increases until the hydrodynamic pressure balances with the normal loading from the sprung platform. For each pad bearing (particularly pads 2 and 3) there is a critical speed below which the film thickness appears to have a relatively constant value of around 1 μm. This is believed to be the speed at which sufficient hydrodynamic load support is generated to balance the initial applied load. This implies that the boundary friction that occurs below this speed is quite low. A maximum film thickness of approximately 10 μm is observed for each of the structured pads. A considerably thinner film is present for the flat-on-flat set-up. This is presumably because the flat specimens have no converging geometry to generate load support. The small film thickness measured for the flat on flat set-up is probably due to the film viscosity wedge effect described by Cameron [11].

4. Conclusions

A new tribometer has been developed to measure the friction in MEMS in representative conditions. The results suggest that the lubricant used operates in the hydrodynamic regime. It is found that structured surfaces with step bearing pads generate thicker lubricant film and exhibit lower friction than completely flat surfaces. Comparison of experimental results with a finite difference solution of Reynolds equation is the subject of ongoing work.

Acknowledgements

The authors wish to thank all members of the Tribology Group in the Department of Mechanical Engineering and the Optical and Semiconductor Devices Group in the Department of Electrical and Electronic Engineering at Imperial College for their help and support over the course of the project.

References

[1] Bennewitz R. Friction force microscopy, fundamentals of friction and wear on the nanoscale. Berlin: Springer; 2007. p. 1–14.
[2] Chen Q, Carman GP. Microscale tribology (friction) measurement and influence of crystal orientation and fabrication process, in: Proceedings of 13th IEEE conference on micro electro mechanical systems (MEMS-2000), January 23–27; 2000. p. 657–1.
[3] Desai AV, Haque MA. A novel MEMS nano-tribometer for dynamic testing in-situ in SEM and TEM. Tribology Letters 2004;17:951–7.
[4] Varenberg M, Peressadko A, Gorb S, Arzt E. Advanced testing of adhesion and friction with a microtribometer. Review of Scientific Instruments 2006;77:066105.
[5] Houston MR, Howe RT, Maboudian R. Effect of hydrogen termination on the work of adhesion between rough polycrystalline silicon surfaces. Journal of Applied Physics 1997;81:3474–83.
[6] Maboudian R, Ashurst WR, Carraro C. Self-assembled monolayers as anti-stiction coatings for MEMS: characteristics and recent developments. Sensors and Actuators A 2000;82:219–23.
[7] Asay DB, Dugger MT, Kim SH. In-situ vapor-phase lubrication of MEMS. Tribology Letters 2008;29(1):67–74.
[8] Deng K, Ramanathan GP, Mehregany M. Micromotor dynamics in lubricating fluids. Journal of Micromechanics and Microengineering 1994;4:266–9.
[9] Mehregany M, Dhuler VR. Operation of electrostatic micromotors in liquid environments. Journal of Micromechanics and Microengineering 1992;2:1–3.
[10] Nainaparampil JJ, Eapen KC, Sanders JH, Voevodin AA. Ionic-liquid lubrication of sliding MEMS contacts: comparison of AFM liquid cell and device-level tests. Journal of Microelectromechanical Systems 2007;16(4):836–43.
[11] Cameron A. The viscosity wedge. ASLE Transactions 1958;1:248–53.